Journal of Electronic Materials (2023) 52:1347–1356
https://doi.org/10.1007/s11664-022-10084-0

ORIGINAL RESEARCH ARTICLE

Surface-Engineered TiO_2 for High-Performance Flexible Supercapacitor Applications

Abdelnaby M. Elshahawy[1] · Saeid M. Elkatlawy[2] · Mustafa S. Shalaby[3] · Cao Guan[4] · John Wang[5]

Received: 7 March 2022 / Accepted: 9 November 2022 / Published online: 4 December 2022

Abstract

Titanium dioxide (TiO_2) shows excellent pseudocapacitive properties. However, the low internal conductivity of TiO_2 limits its use in supercapacitor applications. Therefore, an efficient surface engineering process was developed to enhance the overall pseudocapacitive performance of rutile TiO_2 nanorods. Specifically, surface-engineered TiO_2 nanorod arrays coordinated on carbon cloth were established through the Kapton tape-assisted hydrothermal route. X-ray diffraction analysis confirmed the formation of a tetragonal TiO_2 rutile phase. Morphological analysis revealed the formation of uniform nanorods with an apparent high surface-to-volume aspect ratio. X-ray photoelectron spectroscopy analysis showed that the TiO_2 synthesized in the presence of Kapton tape and annealed under air had high content of hydroxyl groups and Ti^{3+}, which is favorable for supercapacitor performance. Surface treatment of the samples led to significantly enhanced conductivity and electrochemical behavior of TiO_2. The surface-engineered TiO_2 nanorod arrays show specific capacitance of about 57.62 mF/cm^2 at 10 mV/s in 2 M KOH, with excellent rate capability of about 83% at 200 mV/s, and also exhibit long cycle life, retaining 91% of their original capacitance after 10,000 charge/discharge cycles, which is among the highest values reported for TiO_2-based supercapacitors.

Graphical Abstract

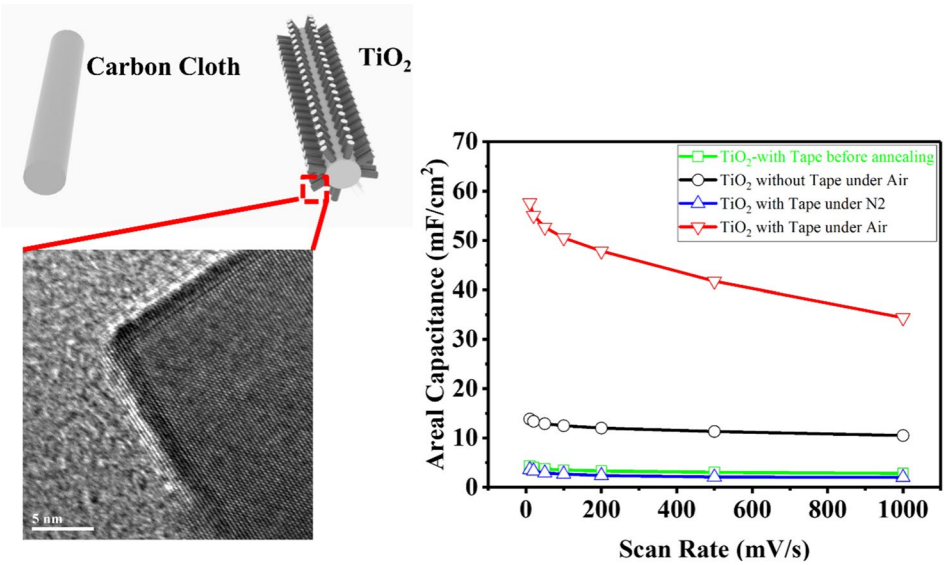

Keywords Rutile TiO_2 · pseudocapacitance · surface engineering · nanorod arrays · supercapacitor

✉ Abdelnaby M. Elshahawy
a.elshahawy@science.aun.edu.eg

Extended author information available on the last page of the article

Introduction

Nowadays, our lives are strongly dependent on portable and wearable devices, including mobile phones, laptops, and electrical-powered transportation utilities. In addition, fossil fuels are being rapidly depleted, contributing to severe environmental pollution.[1,2] Thus, researchers are ramping up their efforts to develop efficient energy storage and conversion devices, such as metal ion batteries and supercapacitors. Supercapacitors are unique due to their large power density and outstanding long-life stability. Similar to metal ion batteries, electrochemical capacitors consist of two electrochemical active electrodes separated by an electrolyte.[3] Based on the charge storage mechanism, supercapacitor electrode materials can be divided into three types: (i) The electric double-layer capacitor (EDLC) electrode, in which the charge can be non-faradaic stored such as graphene, carbon nanotubes, and activated carbon. The charge is electrostatically adsorbed at the electrode–electrolyte interface. (ii) Pseudocapacitive electrodes, for instance, MnO_2, RuO_2, and conductive polymers. The charge in this type can be stored through fast and reversible faradaic reactions at the surface or subsurface of the active electrode material for metal oxides or through doping or de-doping when the polymer is in use. In both EDLC and pseudocapacitive electrodes, the charge is directly proportional to the potential difference and the cyclic voltammetry curves, having either a rectangular or semi-rectangular shape. Moreover, they show high power density. (iii) Battery-type electrodes such as metal hydroxides, metal oxides, metal sulfides, and metal phosphides, in which the charge can be stored through faradaic reaction. The cycle voltammetry and charge/discharge curves are distinguished by pairs of peaks and plateaus, respectively, associated with the redox reactions involved, and thus it can supply large capacity.[4–8]

Battery-type electrodes such as $Ni(OH)_2$, Co_3O_4, and $NiCo_2O_4$ work in basic electrolytes, such as KOH. In addition, these electrode materials face many problems such as aggregation, lack of charge transfer, and difficulties in electrolyte ion diffusion. Thus, it is important to introduce backbone materials with suitable morphology and electrochemical properties that can work in basic electrolytes to enhance the performance of battery-type electrodes.

Among different metal oxides titanium dioxide (TiO_2) has received considerable attention in a wide range of applications due to its unique properties. For instance, TiO_2 has been used in solar energy conversion, memristors, water treatment, and photocatalytic water spitting due to its high reflective index and ability to absorb ultraviolet (UV) light.[9–12] However, there are three different phases—rutile, anatase, and brookite—for TiO_2. Anatase TiO_2 has been widely used in energy storage applications including metal ion batteries.[13–15] TiO_2 shows low specific capacitance of about 330 mAh/g and low volume expansion through a lithiation and delithiation process, which leads to enhanced rate capability and cycle life stability, and thus it has been used as an anode in lithium-ion batteries.[16] TiO_2 is further used in supercapacitors, where engineering of the surface charge of TiO_2 nanotube arrays on Ti foil provided high specific capacitance of about 1.6 mF/cm^2 at a scan rate of 1 mV/s in 1 M NaOH, with 97% capacitance retention after 1000 cycles. This improved performance can be attributed to the presence of Ti^{3+}, which enhances the electrical conductivity of TiO_2.[17] Furthermore, controlling the phase transition of TiO_2 leads to enhanced electrochemical performance, as reported by Salari et al.,[18] who found that the change from anatase to rutile could overcome the charge transfer resistance. Thus, the capacitive behavior was improved, with specific capacitance of about 2.6 mF/cm^2 at a scan rate of 1 mV/s in 1 M NaOH. To further improve the capacitive behavior of TiO_2, Zhou and his research team annealed TiO_2 under hydrogen. They found that dealloying was induced in the presence of a hydrogen atmosphere, leading to the formation of Ti^{3+}, which improved conductivity. The hydrogenated TiO_2 showed specific capacitance of 1.2 mF/cm^2 at 2 mV/s in 0.5 M Na_2SO_4 with rate capability of 58% at 1000 mV/s.[19] Meanwhile, the surface modification of TiO_2 can be used as a backbone in a hierarchical core–shell structure. For instance, Ke et al.[20] fabricated a surface-charged hydrogenated TiO2@$Ni(OH)_2$ core–shell heterostructure. They reported good enhancement of the supercapacitive performance compared to $Ni(OH)_2$ alone. The specific capacity was around 306 mAh/g at 1 mV/s in 6 M KOH, which is higher than that of bare $Ni(OH)_2$, (~200 mAh/g) with 65% rate capability at 100 mV/s. They attributed such performance to the negative surface charge of TiO_2 which helps in the growth of TiO_2 thin nanosheets; thus, more active sites participated in the electrochemical performance. Core–shell or clustered nanostructures of TiO_2/RuO_2 was reported by Park and his team.[21] Due to the synergistic effect between TiO_2 and RuO_2, they achieved high specific capacitance of around 1200 F/g at 1A/g in 1 M H_2SO_4, which is twice as high as that of bare RuO_2.

Based on the results discussed above, TiO_2 nanomaterials show promising properties in supercapacitor applications by modifying their surface charge and/or changing the morphology, leading to enhanced conductivity and surface area, which are key factors for high-performance supercapacitors. Thus, we have designed a low-cost process to modify the surface charge of TiO_2. The process involves the growth of TiO_2 nanorod arrays on carbon cloth with the assistance of Kapton tape, followed by annealing at 550°C. This process aims to (1) modify the surface of TiO_2 by increasing the density of hydroxyl groups on the nanorod arrays after the annealing process, and (2) create a higher amount of Ti^{3+}

on the surface of the nanorods, thus enhancing the conductivity of the electrode materials. Specifically, the TiO_2 with tape annealed under air showed higher Ti^{3+} content and capacitive improvement of 160% compared to the sample annealed under a nitrogen atmosphere, with 91% retention after 10,000 cycles. This pseudocapacitive performance represents one of the best foundations for TiO_2-based electrode materials. Moreover, the new routes for synthesizing surface-engineered TiO_2 nanorod arrays can be applied to a wide range of energy storage materials.

Experimental Section

Preparation of Self-Supported Surface-Engineered TiO_2

Surface engineering of a material can be performed either by depositing a thin film with the required characteristics or by chemical modification of the material. This treatment is aimed at modifying the microstructure and/or the composition of the region near the surface. In this work, the growth of TiO_2 nanorod arrays on carbon cloth (CC) was achieved according to a previous report.[20] Surface modification was performed by chemical treatment. Specifically, 15 ml of HCl at 37% concentration was added to 15 ml deionized (DI) water, and then 1.5 ml of titanium butoxide was added to the acid solution under continuous stirring. The mixture was subsequently transferred into a 50 ml polytetrafluoroethylene (PTFE)-lined stainless steel autoclave, and the hydrothermal process was performed at 150°C for 9 h. After cooling to room temperature, the obtained TiO_2 nanorod arrays were collected, washed with DI water, and dried at 65°C in the oven overnight. For the annealing process, the dried film was placed in a tube furnace and annealed at 550°C for 2 h under an air/N_2 atmosphere.[22]

Characterization

Various characterization techniques were employed to investigate the different properties of TiO_2 nanorod arrays grown on carbon cloth (CC). XRD (Bruker D8 Advance, Cu Kα, λ = 0.154 nm) was used to check the phase formation, and the morphological properties were assessed using scanning electron microscopy (SEM; Zeiss Supra 40) and transmission electron microscopy (TEM; JEOL 2010F at 200 kV). Analysis of the oxidation states and surface properties was established by x-ray photoelectron spectroscopy (XPS) (Kratos Axis Ultra delay-line detector [DLD]), and the spectra were calibrated using a carbon spectrum as a reference).

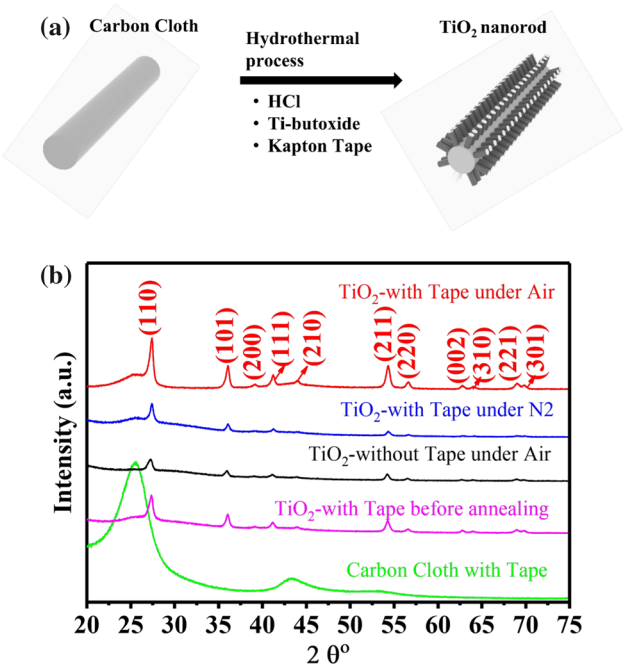

Fig. 1 (a) Schematic illustration of the fabrication of TiO_2 nanorod arrays on carbon cloth; (b) XRD of TiO_2 under different conditions.

Electrochemical Performance Measurements

A 1 cm × 1 cm piece of TiO_2@CC was used as the working electrode, while the reference and counter electrodes were Ag/AgCl and Pt, respectively; 2 M KOH aqueous solution was used as an electrolyte. The three-electrode cell configuration was used to investigate the pseudocapacitive performance of different samples in terms of cyclic voltammetry (CV), galvanostatic charge–discharge measurement, cyclic stability, and electrochemical impedance spectroscopy (EIS) (the frequency for the impedance test was varied from 10^6 to 0.1 Hz, 10 mV). All measurements were carried out with the Solartron 1470E and 1400A system.

The specific capacitance was calculated based on the total mass of the electrode, according to the following equation:

$$C\left(F/cm^2\right) = \frac{\Delta Q}{A\Delta V} \quad (1)$$

where C is the specific capacitance of the electrode in the three-electrode configuration, $(\Delta Q/\Delta V)$ is the slope of the discharge curve after the voltage drop, and A is the area of the electrode.

Results and Discussion

The fabrication process of the self-supported TiO_2 nanorod arrays on carbon cloth is schematically displayed in Fig. 1a. Essentially, TiO_2 nanorods are grown on one side of carbon cloth while the other side is covered with Kapton tape, using the hydrothermal method, and annealing of different samples is then carried out under air or N_2 atmosphere for different samples at 550 °C for 2 h (as described in the experimental section).

Figure 1b shows the XRD patterns for all TiO_2-based samples. All diffraction peaks from all samples at $2\theta = 27.4°$, 36°, 39°, 41.2°, 44°, 54.4°, 56.6°, 62.8°, 64°, 69°, and 69.8°, corresponding to (110), (101), (200), (111), (210), (211), (220), (002), (310), (301), and (112) diffraction planes, respectively, are highly consistent with the tetragonal TiO_2 rutile phase (PDF Card No. 00-021-1276). Additionally, the diffraction peak detected around 26° is clearly attributable to the carbon cloth.[23,24] However, the pattern for the sample annealed under nitrogen shows very weak diffraction peaks in the 2θ range from 60° to 75°, which may be attributed to the lack of oxygen atoms, as will be later assessed by XPS data. The pattern for the sample annealed under air shows strong peaks characteristic of the rutile phase. Generally, the peaks are stronger than those of other samples, which could indicate high crystallinity of this sample in these annealing conditions.

The morphological properties of different TiO_2-based samples were investigated using SEM. TiO_2 nanorod arrays were grown uniformly on the entire surface of carbon cloth fibers, as indicated in the low-magnification SEM images of different TiO_2-based samples, which are shown in the insets of Fig. 2a, b, and c. In addition, the SEM micrographs indicate that the samples possess a high surface-to-volume aspect ratio. The high-magnification SEM images together with the TEM image shown in Figure S1 reveal that the rods are several micrometers in length and about 150–400 nm in diameter. The structural details of the different samples were further established by high-resolution TEM as shown in Fig. 2d, e, and f. The detected interplanar spacing of about 0.32 nm belongs to the (110) plane of rutile TiO_2 (PDF Card No. 00-021-1276).

XPS was carried out to clarify the influence of surface treatment in the presence of Kapton tape and the annealing conditions on the surface composition and to assign the balance state of the different TiO_2 samples (Fig. 3). Figure 3a shows the Ti 2p spectra of different TiO_2-based samples. There are two main peaks located at 464.9 and 459 eV on average, corresponding to Ti $2p_{3/2}$ and Ti $2p_{1/2}$, together with the separation in binding energy between the two

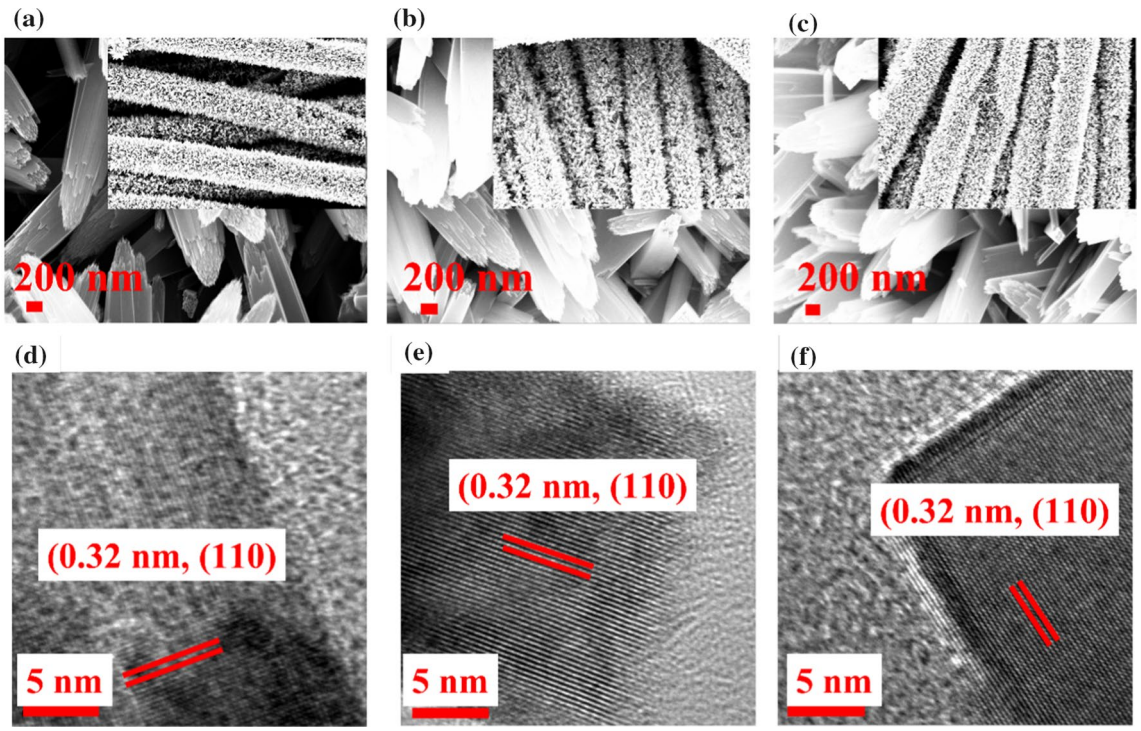

Fig. 2 SEM image of (a) TiO_2 with tape under N_2, (b) TiO_2 without tape under air, (c) TiO_2 with tape under air; high-resolution TEM images of (d) TiO_2 with tape under N_2, (e) TiO_2 without tape under air, (f) TiO_2 with tape under air.

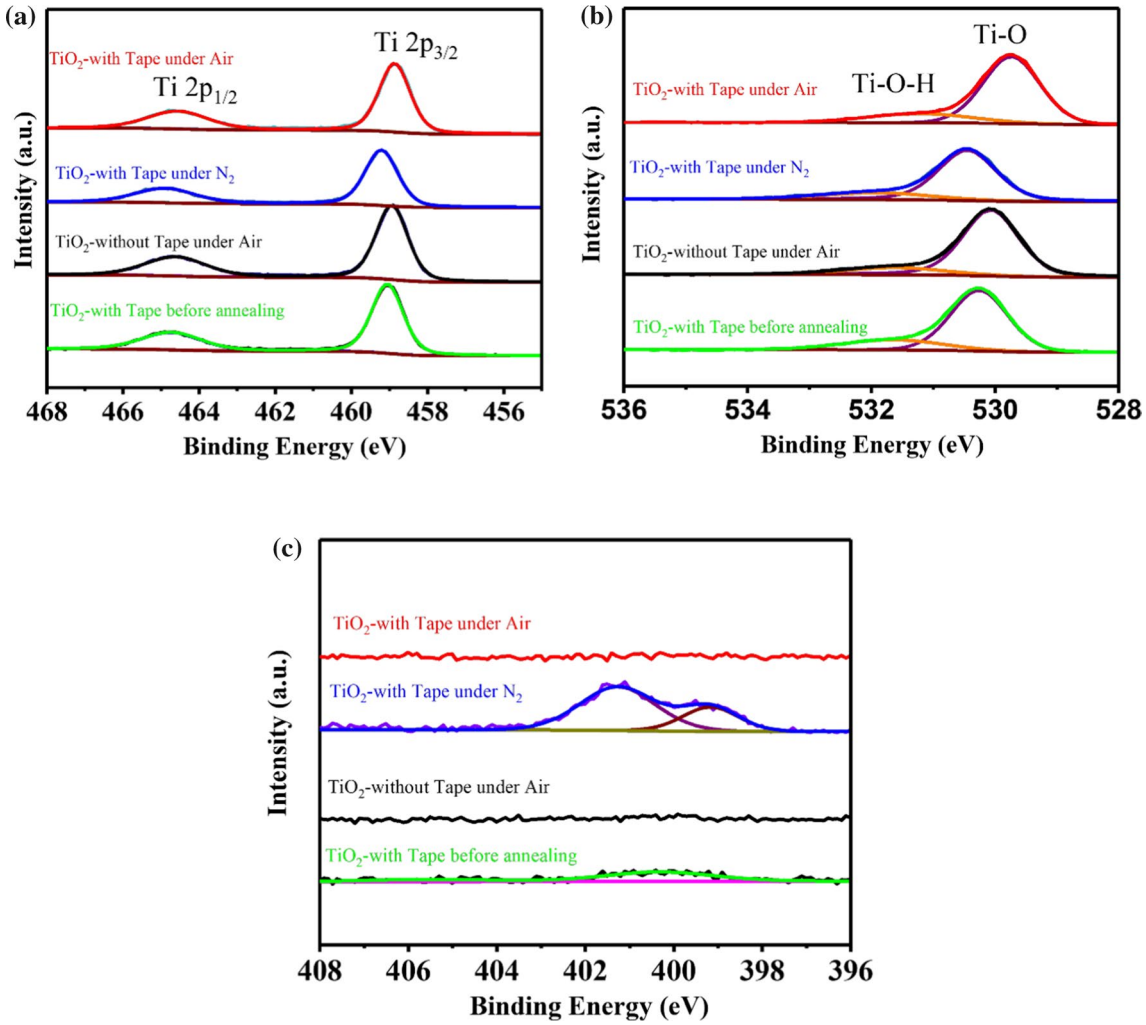

Fig. 3 XPS spectra of TiO_2 (a) Ti 2p, (b) O 1s, (c) N 1s of different samples.

main peaks found to be 5.7 eV corresponding to TiO_2. Even more, there is a small shift towards lower binding energy for the sample of TiO_2 with tape annealed under air, indicating the presence of a small fraction of Ti^{3+} on the surface of TiO_2 nanorod.[25–27] XPS spectra of O 1s are shown in Fig. 3b. The peak around 530.26 eV arises from the formation of metal–oxygen linkage (Ti-O-Ti) and the peak around 531.7 eV can be attributed to the presence of the hydroxyl group as Ti-OH, indicating the surface functionalization by the OH group. The Ti-OH to Ti-O-Ti peaks ratio is found to be 23%, 8%, 20%, and 10% for TiO_2 with tape before annealing, TiO_2 without tape annealed under air, TiO_2 with tape annealed under N_2, and TiO_2 with tape annealed under air, respectively, compared to O 1s. Furthermore, it is noted that for a sample of TiO_2 with tape annealed under air, the Ti-O-Ti bonding peak is shifted to lower binding energy at 529.7 eV, which suggests the existence of Ti^{3+}. The surface modification with the hydroxyl group and the presence of Ti^{3+} is beneficial for pseudocapacitive behavior.[21,28,29] The oxidation state of N in all samples is displayed in Fig. 3c. The N 1s is only detected in TiO_2 with tape before annealing and TiO_2 with tape annealed under N_2 which may respectively come from the desorption of polyamide and carbonized polyamide on the surface of TiO_2 nanorods in the two samples. Additionally, the absence of N 1s in the sample of TiO_2 with tape annealed under air may lead to the formation of oxygen vacancies.[30]

The influence of Kapton tape and annealing conditions on the electrochemical performance of TiO_2 as a cathode is examined using the three-electrode configuration with 2 M KOH as an electrolyte, as depicted in Fig. 4 and Figures S2–S4. The cyclic voltammetry at different scan rates of TiO_2 with tape under air is shown in Fig. 4a, in which the presence of the semi-rectangular shape of CV curves confirms the pseudocapacitive behavior of TiO_2. Figure 4b displays the charge and discharge curves of TiO_2 with tape under air at different current densities. Figure 4b reveals the nearly symmetrical and linear behavior suggesting the high

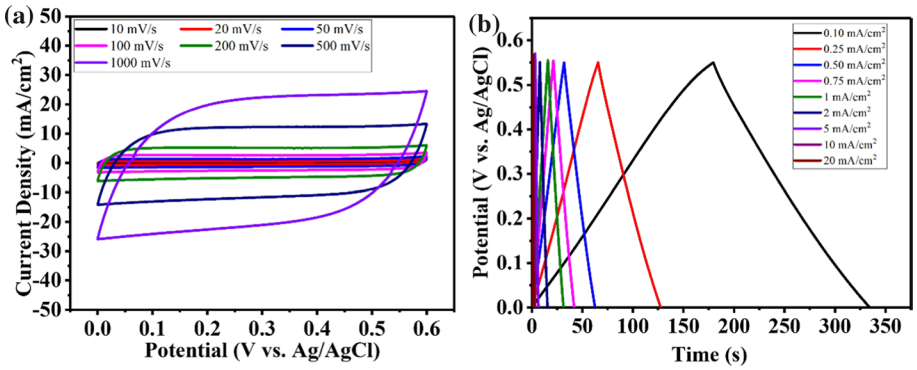

Fig. 4 (a) Cyclic voltammetry curves at different scan rates, and (b) charge/discharge curves at different current densities of TiO_2 with tape under air.

coulombic efficiency and rate capability, which is favorable for supercapacitors. Additionally, one can distinguish between a supercapacitor and a battery as follows: (1) the charge and discharge potentials show a plateau with time because of the formation of different phases for batteries, while they are linear time-dependent for a supercapacitor; (2) batteries show redox peaks with potential difference separation in the cyclic voltammetry curve, whereas the CV curves appear as rectangular or semi-rectangular for a supercapacitor.[31]

A comparison of the electrochemical behavior of TiO_2 with tape before annealing, TiO_2 with tape under N_2, TiO_2 with tape under air, and TiO_2 with tape under air was investigated. As shown in Fig. 5a, the CV curves of different samples at a scan rate of 200 mV/s reveal that the TiO_2 with tape and annealed under air shows the highest current density among the samples, suggesting an improvement in the energy storage capability. Additionally, the symmetrical charge–discharge curves with small IR drops. The TiO_2 sample with tape under air is still able to charge/discharge even at higher current density of about 20 mA/cm^2 compared with other samples, indicating improved ionic/electronic conductivity and enhanced electroactive properties of TiO_2, as shown in Fig. 5b. Moreover, the energy storage in TiO_2 may result from the cation intercalation and de-intercalation processes according to the following mechanism:

$$\left(TiO_2\right)_{Surface} + H_3O^+ + e^- \leftrightarrow \left(TiO_2^- H_3O^+\right)_{Surface} \quad (2)$$

Through the charge/discharge process, the H_3O^+ ions from the electrolyte can intercalate/de-intercalate into TiO_2 nanorods, which contributes to the electrochemical performance. The engineered surface of TiO_2 is another factor that enhances its capacitive properties, due to surface roughness that improves the surface wettability of the electrode and enhances the adsorption of electrolyte ions into the TiO_2.

The specific capacitance as a function of scan rate for different samples is shown in Fig. 5c. The TiO_2 with tape under air shows specific areal capacitance of about 57.6 mF/cm^2 at a scan rate of 10 mV/s, whereas specific capacitance values of about 4.4 mF/cm^2, 13.9 mF/cm^2, and 3.6 mF/cm^2 are reported for TiO_2 with tape before annealing, TiO_2 without tape under air, and TiO_2 with tape under N_2 at the same scan rate, respectively. Moreover, the TiO_2 with tape under air can maintain 60% of its original specific capacitance even at a faster scan rate of 1000 mV/s. Among the different samples, TiO_2 with tape under air exhibits the lowest resistivity, as shown in the Nyquist plot in Fig. 5d.

For further explanation, the equivalent resistance (R_S), which is the sum of the electrolyte ionic resistance, the electronic resistance of the electrode materials, and interface resistance, can be calculated from the interception with the real axis. Another important resistance is the charge transfer resistance (R_{CT}), which indicates the electrode/electrolyte interface resistance. The measured electrochemical impedance for different samples was fitted based on the equivalent circuit, as shown in Fig. 5d, where R_S is equivalent resistance, C_{DL} is double-layer capacitance, W_o is the Warburg diffusion element, R_{CT} is charge transfer resistance, and C_F is the faradaic capacitance. The obtained values are summarized in Table I. It can be seen that the values of R_S are (1.7, 2.06, 1.88, and 2.36) ohms while R_{CT} values are (1.34, 1.19, 0.76, and 1.05) ohms for TiO_2 with tape before annealing, TiO_2 without tape under air, TiO_2 with tape under air, and TiO_2 with tape under N_2, respectively. The lower resistance values (R_{eq} and R_{CT}) for TiO_2 with tape under air indicate better conductivity and capacitive behavior. Furthermore, the Warburg impedance (W_o) of TiO_2 with tape under air shows that the TiO_2 with tape under air is convenient for ion accessibility. The cycling life stability of TiO_2 with tape under air was tested using a charge/discharge test at 0.75 mA/cm^2. As presented in Fig. 5e, the TiO_2 with tape under air preserved 90% of its original specific capacitance after 10,000 charge/discharge cycles. This may be attributed to the enhancement in its conductivity, charge transfer, and ion diffusion.

TiO_2 with tape under air demonstrated significantly better electrochemical performance when compared with other TiO_2-based active materials, which is reported as a backbone for supercapacitor electrode materials, as shown

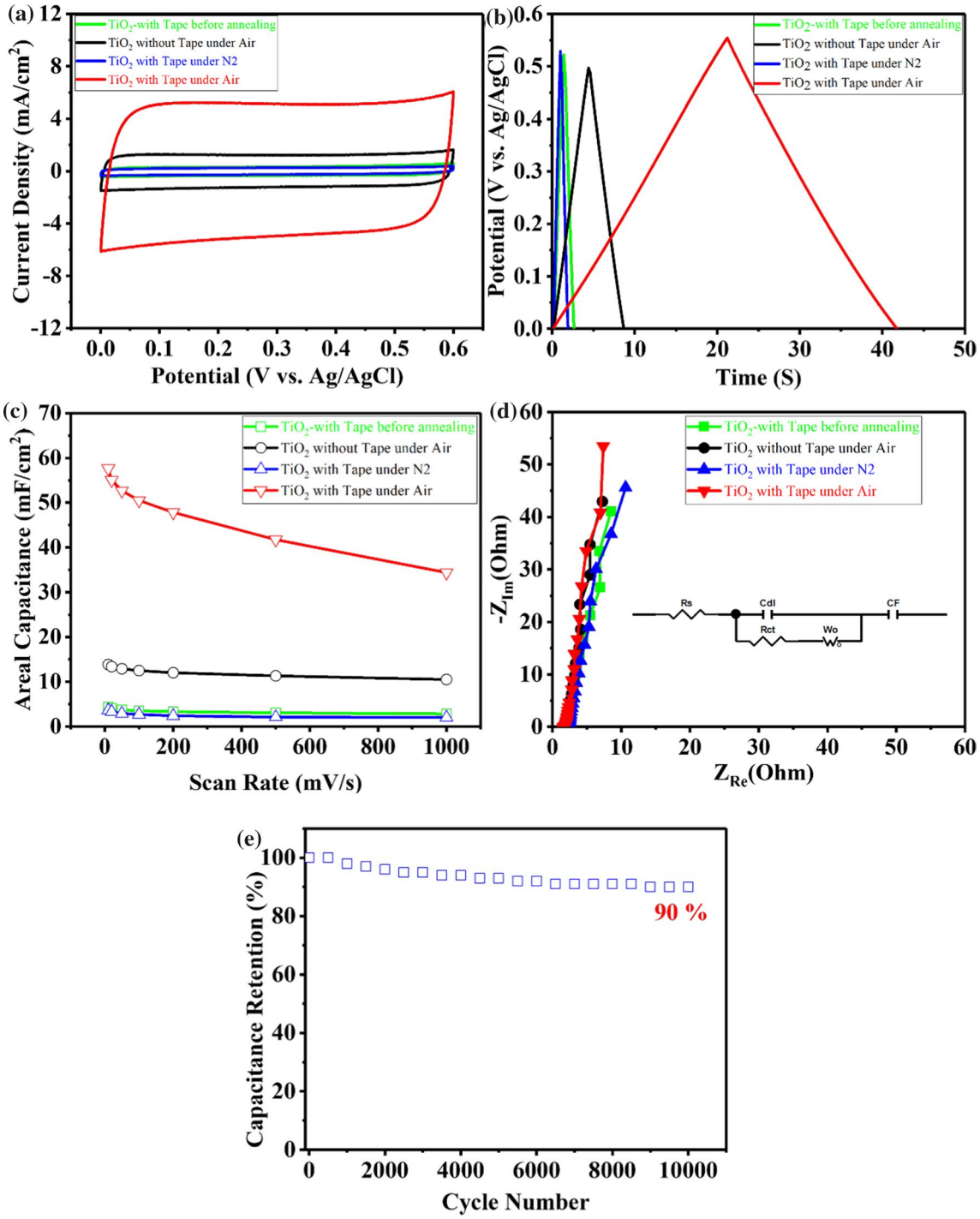

Fig. 5 (a) CV curves at 200.0 mV/s, (b) galvanostatic charge/discharge curves at 0.75 mA/cm^2, (c) specific capacitance as a function of scan rate, (d) EIS plots of TiO_2 with tape before annealing, TiO_2 with tape under N2, TiO_2 without tape under air, and TiO_2 with tape under air; (e) cycling stability of TiO_2 at current density of 0.75 mA/cm^2.

in Table II. For a detailed comparison, Fornasini et al.[32] fabricated TiO_2 nanoparticles with reduced graphene oxide in situ using the LightScribe® technique. Their micro-supercapacitor achieved specific capacitance of about 10 mF/cm^2 at current density of 5 μA/cm^2 in polyvinyl alcohol/H_2SO_4, and retained 72% of its original capacitance after 3000 charge/discharge cycles. Blue TiO_2 nanosheets demonstrated specific areal capacitance of ~ 19 mF/cm^2 at 0.5 mA/cm^2 in 1 M Na_2SO_4, with rate capability of 39% at 10 mA/cm^2,[33] whereas TiO2 nanotube arrays grown on

Ti foil demonstrated areal capacitance of 200 mF/cm^2 at current density of 1 mA/cm^2 in 1 M HCl, 90% of which was retained after 5000 cycles at 1 mA/cm^2.[28] Zhang et al.[34] fabricated MoO_3/titania nanotube composites on Ti sheets. They reported areal capacitance of around 3.14 mF/cm^2 for TiO_2 nanotube arrays at a scan rate of 0.6 mA/cm^2 in 2 M Li_2SO_4. Nitridation of a hollow TiO_2 multi-shell at 900°C supplied 7 mF/cm^2 at a scan rate of 50 mV/s, while the monolayer of nitrided titania showed only 0.8 mF/cm^2.[35] K-doped mixed-phase TiO_2 nanofibers supported on Ti foil exhibited 21.45 mF/cm^2 at a scan rate of 500 mV/s in 1 M KOH, with 91% retention of its capacitance at 0.5 mA/cm^2 after 2500 cycles.[29] The TiO_2 with tape under air designed in this work showed areal capacitance of about 27.8 mF/cm^2 at current density of 1 mA/cm^2. Such enhancement in the electrochemical behavior can be attributed to the surface engineering of TiO_2 nanorods by surface functionalization via the hydroxyl group or induced Ti^{3+} through the oxygen voids.

Table I Fitting results for the electrochemical impedance for TiO_2-based active materials

Sample	R_S	R_{CT}	W_o	C_{DL}	C_F
TiO_2 with tape before annealing	1.7	1.34	8.63	0.0006	0.00071
TiO_2 without tape under air	2.06	1.19	7.45	0.0009	0.0015
TiO_2 with tape under air	1.88	0.76	7.86	0.0072	0.0089
TiO_2 with tape under N2	2.36	1.05	4.87	0.00028	0.000086

Conclusions

In summary, we have designed a low-cost strategy to solve the internal resistance and hence the overall electrochemical performance of TiO_2, using a Kapton tape-assisted hydrothermal process. We found that after annealing, the surface of the TiO_2 was modified by increasing the number of hydroxyl groups and Ti^{3+} on the surface. Moreover, the derived surface-engineered TiO_2@CC provides high specific areal capacitance of about 27.8mF/cm^2 at 1 mA/cm^2, with excellent rate capability and long cycle life stability, retaining over 91% of its initial specific capacitance after 10,000 cycles. The overall high pseudocapacitive behavior suggests that the strategy of surface-engineered TiO_2 provides new opportunities for the use of TiO_2 as a backbone in high-performance supercapacitor devices.

Table II Comparison of electrochemical performance of TiO_2-based active materials

References	Materials	Electrolyte	Potential window (V)	Cs (mF/cm^2)	Cycle life
[36]	Hydrogenated TiO_2 nanotubes	0.5 M Na_2SO_4	0–0.8	3.24 mF cm^{-2}@ 100 mV s^{-1}	97% After 10,000 cycles @100 mV/s
[19]	Hydrogenated TiO_2	0.5 M Na_2SO_4	−0.2 to 0.6	1.05@100 mV/s	93.8% after 1000 cycles @0.1 mA/cm^2
[35]	N-TiO_2	1 M Na_2SO_4	0–1	2.48@10 mV/s	88.7% after 1000 cycles @200 mV/s
[37]	Spaced TiO_2 (annealed under NH_3)	0.5 M Na_2SO_4	0–0.8	42.4@200 mV/s, 22.5@1 mA/cm^2	78% after 2000 cycles @3 mA/cm^2
[38]	Solid-state cable-type supercapacitor PEDOT:TiO_2	PVA-LiCl	0–1.1	2.65@0.1 mA/cm	––
[39]	Black TiO_2	1 M Na_2SO_4	0–0.8	15.6@100 mV/s	96% after 5000 cycles @100 mV/s
[40]	TiO_2@C	0.5 M Na_2SO_4	0–0.8	23.6 @5 mV/s	91% after 1000 cycles @1 mA/cm^2
[41]	VO_2@TiO_2	8 M LiCl	−1 to –0.3	13@1000 mV/s	84.3% after 1000 cycles @10A/g
[42]	Self-doped-TiO_2	0.5 M Na_2SO_4	0–1	1.84@5 mV/s	93.1% after 2000 cycles @100 mV/s
[43]	TiO_2 at Ti foil	1 MNa_2SO_4	0–0.8	0.86@1 mV/s	98.4% after 1000 cycles @0.1 mA/cm^2
This work	TiO_2 with Kapton tape, annealed under air	2 M KOH	0–0.6	57.62mF/cm^2 @10 mV/s, 47.83mF/cm^2 @200 mV/s 27.8mf/cm^2 @1 mA/cm^2	91% after 10,000 cycles @0.75 mA/cm^2

Supplementary Information The online version contains supplementary material available at https://doi.org/10.1007/s11664-022-10084-0.

Funding Open access funding provided by The Science, Technology & Innovation Funding Authority (STDF) in cooperation with The Egyptian Knowledge Bank (EKB).

Conflict of interest The authors declare that they have no conflict of interest.

References

1. S. Kumar, G. Saeed, L. Zhu, K.N. Hui, N.H. Kim, and J.H. Lee, 0D to 3D carbon-based networks combined with pseudocapacitive electrode material for high energy density supercapacitor: a review. *Chem. Eng. J.* 403, 126352 (2021).
2. A. Mohanty, D. Jaihindh, Y.-P. Fu, S.P. Senanayak, L.S. Mende, and A. Ramadoss, An extensive review on three dimension architectural metal-organic frameworks towards supercapacitor application. *J. Power Sources* 488, 229444 (2021).
3. S. Zhang, and N. Pan, Supercapacitors performance evaluation. *Adv. Energy Mater.* 5, 1401401 (2015).
4. Y. Wang, Y. Song, and Y. Xia, Electrochemical capacitors: mechanism, materials, systems, characterization and applications. *Chem. Soc. Rev.* 45, 5925 (2016).
5. P. Simon, and Y. Gogotsi, Materials for electrochemical capacitors. *Nat. Mater.* 7, 845 (2008).
6. K. Nasrin, S. Gokulnath, M. Karnan, K. Subramani, and M. Sathish, Redox-additives in aqueous, non-aqueous, and all-solid-state electrolytes for carbon-based supercapacitor: a mini-review. *Energy Fuels* 35, 6465 (2021).
7. Y. Wang, G. Liu, Y. Liu, J. Yang, P. Liu, Q. Jiang, F. Jiang, C. Liu, W. Ding, and J. Xu, Heterostructural conductive polymer with multi-dimensional carbon materials for capacitive energy storage. *Appl. Surf. Sci.* 558, 149910 (2021).
8. L. Ruiyi, H. Keyang, Y. Yongqiang, Z. Haiyan, and L. Zaijun, Atomically dispersed RuO_2-tryptophan functionalized graphene quantum dot-graphene hybrid with double Schottky heterojunctions for high performance flexible supercapacitors. *Chem. Eng. J.* 426, 130893 (2021).
9. A. Gupta, K. Sahu, M. Dhonde, and V.V.S. Murty, Novel synergistic combination of Cu/S co-doped TiO_2 nanoparticles incorporated as photoanode in dye sensitized solar cell. *Sol. Energy* 203, 296 (2020).
10. C. Tao, Q. Jia, B. Han, and Z. Ma, Tunable selectivity of radical generation over TiO_2 for photocatalysis. *Chem. Eng. Sci.* 214, 115438 (2020).
11. J. Wu, W. Wang, Y. Tian, C. Song, H. Qiu, and H. Xue, Piezotronic effect boosted photocatalytic performance of heterostructured $BaTiO_3/TiO_2$ nanofibers for degradation of organic pollutants. *Nano Energy* 77, 105122 (2020).
12. S. Cao, T.-S. Chan, Y.-R. Lu, X. Shi, B. Fu, Z. Wu, H. Li, K. Liu, S. Alzuabi, P. Cheng, M. Liu, T. Li, X. Chen, and L. Piao, Photocatalytic pure water splitting with high efficiency and value by Pt/porous brookite TiO_2 nanoflutes. *Nano Energy* 67, 104287 (2020).
13. W. Mao, W. Yue, Z. Xu, J. Wang, J. Zhang, D. Li, B. Zhang, S. Yang, K. Dai, G. Liu, and G. Ai, Novel hoberman sphere design for interlaced Mn_3O_4@CNT architecture with atomic layer deposition-coated TiO_2 overlayer as advanced anodes in li-ion battery. *ACS Appl. Mater. Interfaces* 12, 39282 (2020).
14. L. Yu, L. Zhang, J. Fu, J. Yun, and K.H. Kim, Hierarchical Tiny-Sb encapsulated in MOFs derived-carbon and TiO_2 hollow nanotubes for enhanced Li/Na-Ion half-and full-cell batteries. *Chem. Eng. J.* 417, 129106 (2021).
15. Q. Wang, L. Shen, T. Xue, G. Cheng, C.Z. Huang, H.J. Fan, and Y.P. Feng, Single-crystalline TiO_2(B) nanobelts with unusual large exposed 100 facets and enhanced li-storage capacity. *Adv. Funct. Mater.* 31, 2002187 (2021).
16. Z. Xiao, C. Yu, X. Lin, X. Chen, C. Zhang, H. Jiang, R. Zhang, and F. Wei, TiO_2 as a multifunction coating layer to enhance the electrochemical performance of SiOx@TiO_2@C composite as anode material. *Nano Energy* 77, 105082 (2020).
17. M. Salari, S.H. Aboutalebi, A.T. Chidembo, K. Konstantinov, and H.K. Liu, Surface engineering of self-assembled TiO_2 nanotube arrays: a practical route towards energy storage applications. *J. Alloy. Compd.* 586, 197 (2014).
18. M. Salari, S.H. Aboutalebi, A.T. Chidembo, I.P. Nevirkovets, K. Konstantinov, and H.K. Liu, Enhancement of the electrochemical capacitance of TiO_2 nanotube arrays through controlled phase transformation of anatase to rutile. *Phys. Chem. Chem. Phys.* 14, 4770 (2012).
19. H. Zhou, Y. Zhong, Z. He, L. Zhang, J. Wang, J. Zhang, and C.-N. Cao, Three-dimensional nanoporous TiO_2 network films with excellent electrochemical capacitance performance. *J. Alloy. Compd.* 597, 1 (2014).
20. Q. Ke, C. Guan, X. Zhang, M. Zheng, Y.-W. Zhang, Y. Cai, H. Zhang, and J. Wang, Surface-charge-mediated formation of H-TiO_2@$Ni(OH)_2$ heterostructures for high-performance supercapacitors. *Adv. Mater.* 29, 1604164 (2017).
21. S. Park, D. Shin, T. Yeo, B. Seo, H. Hwang, J. Lee, and W. Choi, Combustion-driven synthesis route for tunable TiO_2/RuO_2 hybrid composites as high-performance electrode materials for supercapacitors. *Chem. Eng. J.* 384, 123269 (2020).
22. Q. Ke, M. Zheng, H. Liu, C. Guan, L. Mao, and J. Wang, 3D TiO_2@$Ni(OH)_2$ core-shell arrays with tunable nanostructure for hybrid supercapacitor application. *Sci. Rep.* 5, 13940 (2015).
23. A.M. Elshahawy, C. Guan, X. Li, H. Zhang, Y. Hu, H. Wu, S.J. Pennycook, and J. Wang, Sulfur-doped cobalt phosphide nanotube arrays for highly stable hybrid supercapacitor. *Nano Energy* 39, 162 (2017).
24. P. Rani, A. Ghorai, S. Roy, D.K. Goswami, A. Midya, and S.K. Ray, Mesoporous GO-TiO_2 nanocomposites for flexible solid-state supercapacitor applications. *Mater. Res. Express* 6, 125546 (2020).
25. D. Shin, J. Shin, T. Yeo, H. Hwang, S. Park, and W. Choi, Scalable synthesis of triple-core–shell nanostructures of TiO_2@MnO_2@C for high performance supercapacitors using structure-guided combustion waves. *Small* 14, 1703755 (2018).
26. V.H. Pham, T.-D. Nguyen-Phan, X. Tong, B. Rajagopalan, J.S. Chung, and J.H. Dickerson, Hydrogenated TiO_2@reduced graphene oxide sandwich-like nanosheets for high voltage supercapacitor applications. *Carbon* 126, 135 (2018).
27. W. Fu, E. Zhao, R. Ma, Z. Sun, Y. Yang, M. Sevilla, A.B. Fuertes, A. Magasinski, and G. Yushin, Anatase TiO_2 confined in carbon nanopores for high-energy li-ion hybrid supercapacitors operating

at high rates and subzero temperatures. *Adv. Energy Mater.* 10, 1902993 (2020).
28. C.C. Raj, V. Srimurugan, A. Flamina, and R. Prasanth, Tuning the carrier density of TiO_2 nanotube arrays by controlling the oxygen vacancies for improved areal capacitance in supercapacitor applications. *Mater. Chem. Phys.* 248, 122925 (2020).
29. H.R. Barai, M.M. Rahman, and S.W. Joo, Annealing-free synthesis of K-doped mixed-phase TiO_2 nanofibers on Ti foil for electrochemical supercapacitor. *Electrochim. Acta* 253, 563 (2017).
30. J. Yu, M. Zeng, J. Zhou, H. Chen, G. Cong, H. Liu, M. Ji, C. Zhu, and J. Xu, A one-pot synthesis of nitrogen doped porous MXene/TiO_2 heterogeneous film for high-performance flexible energy storage. *Chem. Eng. J.* 426, 130765 (2021).
31. P. Simon, Y. Gogotsi, and B. Dunn, Where do batteries end and supercapacitors begin? *Science* 343, 1210 (2014).
32. L. Fornasini, S. Scaravonati, G. Magnani, A. Morenghi, M. Sidoli, D. Bersani, G. Bertoni, L. Aversa, R. Verucchi, M. Riccò, P.P. Lottici, and D. Pontiroli, In situ decoration of laser-scribed graphene with TiO_2 nanoparticles for scalable high-performance micro-supercapacitors. *Carbon* 176, 296 (2021).
33. P. Pazhamalai, K. Krishnamoorthy, V.K. Mariappan, and S.-J. Kim, Blue TiO_2 nanosheets as a high-performance electrode material for supercapacitors. *J. Colloid Interface Sci.* 536, 62 (2019).
34. B. Zhang, S. Sun, N. Shi, X. Liao, G. Yin, Z. Huang, X. Chen, and X. Pu, Spaced TiO_2 nanotube arrays for electrodeposition of MoO_3 to achieve high electrochemical performance. *J. Alloy. Compd.* 820, 153066 (2020).
35. G.D. Moon, J.B. Joo, M. Dahl, H. Jung, and Y. Yin, Nitridation and layered assembly of hollow TiO_2 shells for electrochemical energy storage. *Adv. Funct. Mater.* 24, 848 (2014).
36. X. Lu, G. Wang, T. Zhai, M. Yu, J. Gan, Y. Tong, and Y. Li, Hydrogenated TiO_2 nanotube arrays for supercapacitors. *Nano lett.* 12, 1690 (2012).
37. N.T. Nguyen, S. Ozkan, I. Hwang, X. Zhou, and P. Schmuki, Spaced TiO_2 nanotube arrays allow for a high performance hierarchical supercapacitor structure. *J. Mater. Chem. A* 5, 1895 (2017).
38. R. Vellacheri, H. Zhao, M. Mühlstädt, A. Al-Haddad, K.D. Jandt, and Y. Lei, Rationally engineered electrodes for a high-performance solid-state cable-type supercapacitor. *Adv. Funct. Mater.* 27, 1606696 (2017).
39. C. Kim, S. Kim, J. Lee, J. Kim, and J. Yoon, Capacitive and oxidant generating properties of black-colored TiO_2 nanotube array fabricated by electrochemical self-doping. *ACS Appl. Mater. Interfaces* 7, 7486 (2015).
40. H. Tang, M. Xiong, D. Qu, D. Liu, Z. Zhang, Z. Xie, X. Wei, W. Tu, and D. Qu, Enhanced supercapacitive performance on TiO_2@C coaxial nano-rod array through a bio-inspired approach. *Nano Energy* 15, 75 (2015).
41. C. Hu, H. Xu, X. Liu, F. Zou, L. Qie, Y. Huang, and X. Hu, VO_2/TiO_2 nanosponges as binder-free electrodes for high-performance supercapacitors. *Sci. Rep.* 5, 16012 (2015).
42. H. Zhou, and Y. Zhang, Electrochemically self-doped TiO_2 nanotube arrays for supercapacitors. *J. Phys. Chem. C* 118, 5626 (2014).
43. Z. Zheng, J. Chen, R. Yoshida, X. Gao, K. Tarr, Y.H. Ikuhara, and W. Zhou, One-step synthesis of TiO_2nanorod arrays on Ti foil for supercapacitor application. *Nanotechnology* 25, 435406 (2014).

Authors and Affiliations

Abdelnaby M. Elshahawy[1] · Saeid M. Elkatlawy[2] · Mustafa S. Shalaby[3] · Cao Guan[4] · John Wang[5]

[1] Department of Physics, Faculty of Science, Assiut University, Assiut 71516, Egypt

[2] Department of Physics, Faculty of Science, Damanhour University, Damanhour 22111, Egypt

[3] Solid State Physics and Accelerators Department, National Center for Radiation Research and Technology, Egyptian Atomic Energy Authority, Cairo, Egypt

[4] Frontiers Science Center for Flexible Electronics, Institute of Flexible Electronics, Northwestern Polytechnical University, Xi'an 710072, People's Republic of China

[5] Department of Materials Science and Engineering, National University of Singapore, 9 Engineering Drive 1, Singapore 117575, Singapore